

# Potential of mean force for electrical conductivity of dense plasmas

C. E. Starrett<sup>1,\*</sup>

<sup>1</sup>*Los Alamos National Laboratory, P.O. Box 1663, Los Alamos, NM 87545, U.S.A.*

(Dated: February 24, 2022)

The electrical conductivity in dense plasmas can be calculated with the relaxation-time approximation provided that the interaction potential between the scattering electron and the ion is known. To date there has been considerable uncertainty as to the best way to define this interaction potential so that it correctly includes the effects of ionic structure, screening by electrons and partial ionization. Current approximations lead to significantly different results with varying levels of agreement when compared to bench-mark calculations and experiments. We present a new way to define this potential, drawing on ideas from classical fluid theory to define a potential of mean force. This new potential results in significantly improved agreement with experiments and bench mark calculations, and includes all the aforementioned physics self-consistently.

Keywords: electrical conductivity

## I. INTRODUCTION

Accurate prediction of electronic conductivity in dense plasmas has proved to be a challenging problem. One approach is to use density functional theory molecular dynamics (DFT-MD) coupled with the Kubo-Greenwood formalism [1–6]. This method is thought to be accurate but is limited in the problems it can be applied to due to its significant computational expense. Moreover, fundamental questions like its treatment of electron-electron collisional effects are still active areas of research [6]. Experimentally, the subject is an active area of research [7] and has a long history [8–12], in part due to the difficulty in obtaining model independent measurements.

Another class of methods starts from the Boltzman equation and introduces a relaxation-time approximation [13] in which electrons are scattered from ions and other electrons. The question then becomes one of calculating the electron-ion and electron-electron cross sections. In the degenerate electron limit this approach becomes identical to the famous Ziman method [14, 15].

To calculate the electron-ion cross section in dense plasmas one needs to be able to model partial ionization induced by density and temperature, and also the corresponding changes in the ionic structure. Average atom models have long been used for this purpose [14, 16–21]. They are DFT based models that attempt to calculate the properties of one averaged atom in the plasma. They are computationally efficient and are well suited to making wide ranging tables of data [16].

While on the face of it, it seems natural to couple these average atoms to the relaxation time approximation and thus calculate conductivities, it turns out that the results are sensitive to exactly how this coupling is done. Specifically, one needs to define an electron-ion scattering potential, and how this definition is made strongly effects the resulting conductivities [14, 17, 22, 23].

In this paper we explore a new method of coupling average atom models to the relaxation-time approximation that extends the potential of mean force from classical fluid theory [24] to the quantum domain. Thus, a new quantum potential of mean force is defined. It includes correlations with electrons and ions surrounding the central scatterer through the quantum fluid equations known as the quantum Ornstein-Zernike equations [25]. We find that the new potential leads to generally more accurate conductivity predictions when compared to DFT-MD simulations and experiments for aluminum over a wide range of conditions. We also explore the influence of electron-electron collisions by including a correction factor due to Reinholz *et al* [26], and find that plays a significant and important role in certain cases.

## II. THEORETICAL MODEL

### A. Conductivity in terms of the electron relaxation time

In the relaxation-time approximation the conductivity is given by <sup>1</sup>

$$\sigma_{DC} = \int_0^\infty \left( -\frac{df}{d\epsilon} \right) N_e(\epsilon) \tau_\epsilon d\epsilon \quad (1)$$

where  $\tau_\epsilon$  is the energy dependent relaxation time,  $f$  is the Fermi-Dirac occupation factor,

$$N_e(\epsilon) = n_I^0 \int_0^\epsilon d\epsilon' \chi(\epsilon') \quad (2)$$

\*Electronic address: starrett@lanl.gov

<sup>1</sup> Unless otherwise stated, atomic units are used throughout in which  $\hbar = m_e = e = k_B = a_B = 1$ , and the symbols have their usual meanings.

and  $\chi(\epsilon)$  is the density of states such that the number of valence electrons per atom  $\bar{Z}$  is

$$\bar{Z} = \frac{\bar{n}_e^0}{n_I^0} = \int_0^\infty d\epsilon \chi(\epsilon) f(\epsilon, \mu_e) \quad (3)$$

Here  $\mu_e$  is chemical potential and  $\bar{n}_e^0$  ( $n_I^0$ ) is the density of valence electrons (ions). If we take the density of states to be its free electron form

$$\chi^{free}(\epsilon) = \frac{\sqrt{2\epsilon}}{n_I^0 \pi^2} \quad (4)$$

then

$$N_e^{free}(\epsilon) = \frac{v^3}{3\pi^2} \quad (5)$$

where  $\epsilon = v^2/2$ . The resulting equation that we will use here is

$$\sigma_{DC} = \frac{1}{3\pi^2} \int_0^\infty \left( -\frac{df}{d\epsilon} \right) v^3 \tau_\epsilon d\epsilon \quad (6)$$

### B. The electron relaxation time's relation to the momentum transport cross section

The relaxation time is related to the mean free path  $\lambda_\epsilon$  by

$$\tau_\epsilon = \frac{\lambda_\epsilon}{v} \quad (7)$$

which is in turn related to the momentum transport cross section  $\sigma_{TR}(\epsilon)$

$$\lambda_\epsilon = \frac{1}{n_I^0 \sigma_{TR}(\epsilon)} \quad (8)$$

hence

$$\tau_\epsilon = \frac{1}{n_I^0 v \sigma_{TR}(\epsilon)} \quad (9)$$

### C. The momentum transport cross section in terms of scattering phase shifts

The momentum transport cross section is calculated from

$$\sigma_{TR}(p) = 2\pi \int_0^\pi d\theta \frac{d\sigma}{d\theta}(\epsilon, \theta) (1 - \cos \theta) \sin \theta \quad (10)$$

where  $p = m_e v$  and  $\frac{d\sigma}{d\theta}(\epsilon, \theta)$  is the differential cross section for one scatterer in the plasma. This can be calculated from the scattering phase shifts  $\eta_l(\epsilon)$  once the single center scattering potential  $V^{scatt}(r)$  is known.

$$\frac{d\sigma}{d\theta}(\epsilon, \theta) = |\mathcal{F}(\epsilon, \theta)|^2 \quad (11)$$

where the scattering amplitude  $\mathcal{F}$  is

$$\mathcal{F}(\epsilon, \theta) = \frac{1}{p} \sum_{l=0}^\infty (2l+1) \sin \eta_l e^{i\eta_l} P_l(\cos \theta) \quad (12)$$

The angular integral in equation (10) can be carried out analytically, yielding

$$\sigma_{TR}(\epsilon) = \frac{4\pi}{p^2} \sum_{l=0}^\infty (l+1) (\sin(\eta_{l+1} - \eta_l))^2 \quad (13)$$

### D. Choice of scattering potential

To calculate the scattering amplitude  $\mathcal{F}$  or momentum transfer cross section  $\sigma_{TR}(r)$  we need a scattering potential  $V^{scatt}(r)$ . The physical picture inherent to our application of the relaxation time approximation is that electrons scatter off one center at a time, and that the plasma is made up of identical scattering centers. The question then becomes: what defines a scattering center?

#### 1. Pseudoatom (PA) potential

Lets assume that the plasma is made up of an ensemble of identical pseudoatoms. Each pseudoatom is a nucleus and a spherically symmetric screening cloud of electrons with density  $n_e^{PA}(r)$ . The total potential for the plasma is then

$$V(\mathbf{r}) = \sum_{i=1}^N V^{PA}(|\mathbf{r} - \mathbf{R}_i|) \quad (14)$$

where the sum is over the  $N$  nuclei in the plasma and

$$V^{PA}(r) = -\frac{Z}{r} + \int d^3r' \frac{n_e^{PA}(r')}{|\mathbf{r} - \mathbf{r}'|} + V^{xc}[n_e^{PA}(r)] \quad (15)$$

with  $V^{xc}[n]$  being the contribution from electron exchange and correlation.

In the high energy limit the Born cross section becomes accurate and the scattering cross section for the whole plasma is

$$\frac{d\sigma^{plasma}}{d\theta}(\epsilon, \theta) = \left| \frac{V(\mathbf{q})}{2\pi} \right|^2 \quad (16)$$

where

$$q^2 = 2p^2[1 - \cos \theta] \quad (17)$$

and the Fourier transform of the potential is

$$V(\mathbf{q}) = \int d^3r e^{-i\mathbf{r} \cdot \mathbf{q}} V(\mathbf{r}) \quad (18)$$

Taking the Fourier Transform of equation (14) and using the definition of the ionic structure factor

$$S_{ii}(q) = \frac{1}{N} \langle \rho_{\mathbf{q}} \rho_{-\mathbf{q}} \rangle \quad (19)$$

where

$$\rho_{\mathbf{q}} = \sum_i e^{-i\mathbf{q} \cdot \mathbf{R}_i} \quad (20)$$

and the angular brackets indicate that the configurational average has been taken, the differential cross section per scattering center becomes

$$\frac{d\sigma}{d\theta}(\epsilon, \theta) = S_{ii}(q) \left| \frac{V^{PA}(q)}{2\pi} \right|^2 \quad (21)$$

This is valid when the Born approximation is accurate (i.e. for weak scattering, typically high energy scattering electrons). To return to the strong scatterer picture for which the Born approximation is invalid, one approach [14] is to replace the Born cross section  $|V^{PA}(q)/2\pi|^2$  with its t-matrix equivalent, equations (11) and (12), i.e.

$$\frac{d\sigma}{d\theta}(\epsilon, \theta) = S_{ii}(q) |\mathcal{F}^{PA}(\epsilon, \theta)|^2 \quad (22)$$

where  $\mathcal{F}^{PA}$  is the scattering amplitude for the  $V^{PA}(r)$  potential. However, as the differential cross section now depends on  $S_{ii}(q)$ , the angular integral in equation (10) can longer be done analytically and must be done numerically<sup>2</sup>.

Using this approach the Born limit of the scattering cross section is recovered, and so the method should be accurate at high temperatures or high densities where the scattering electrons have high energies. However, at relatively lower densities and temperatures (like room temperature and pressure), the Born cross section will be significantly in error, and therefore equation (22) may also be significantly in error.

### 2. Average atom (AA) potential

An alternative and routinely used [16, 17, 20, 21, 27–29] definition of the scattering potential is to use an average atom potential  $V^{AA}(r)$ . There are a number of realistic variations on how this should be defined but such variations are relatively unimportant for present purposes. We define

$$V^{AA}(r) = -\frac{Z}{r} + \int_{r < R_{WS}} d^3r' \frac{n_e^{AA}(r')}{|\mathbf{r} - \mathbf{r}'|} + V^{xc}[n_e^{AA}(r)] \quad (23)$$

where the integral and the potential are confined to the ion sphere with (Wigner-Seitz) radius  $R_{WS}$ . The ion-sphere is required to the charge neutral and typically  $V^{AA}(r) = 0$  for  $r > R_{WS}$ . In this approach

$$\frac{d\sigma}{d\theta}(\epsilon, \theta) = S_{ii}(q) |\mathcal{F}^{AA}(\epsilon, \theta)|^2 \quad (24)$$

<sup>2</sup> From a numerical point of view the angular integral in equation (10) is not particularly difficult.

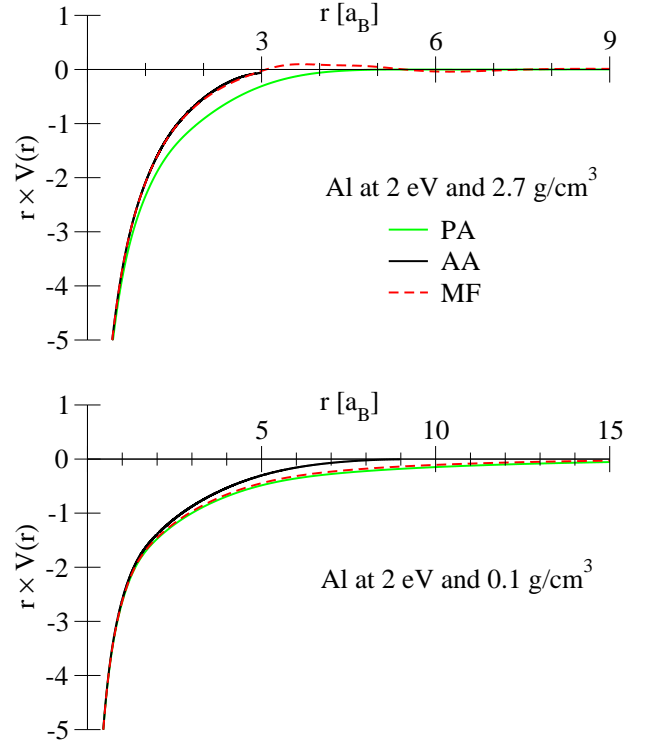


FIG. 1: (Color online) Examples of scattering potentials for two different aluminum cases. In the top panel, for aluminum at 2.7 g/cm<sup>3</sup> and 2 eV, the mean force potential is close to the average atom potential (which only extends to the ion sphere radius). In the bottom panel, for aluminum at 0.1 g/cm<sup>3</sup> and 2 eV, the mean force potential is closer to the pseudoatom potential.

In deriving this result [30] one assumes a muffin-tin potential and a crude estimate of multiple scattering effects gives rise to the ionic structure factor  $S_{ii}(q)$ . The average atom potential  $V^{AA}(r)$  cannot recover the Born limit and equation (24) will be incorrect in the high temperature or high density limit.

### 3. Potential of mean force (MF)

We desire the potential felt by one electron as it scatters from one center. This scattering does not happen in isolation as in the  $V^{PA}(r)$  approximation (equation (22)). For classical (“cl”) particles the Ornstein-Zernike equations can be used to define a potential of mean force that includes the potential created by the central scatterer as well as its correlations with surrounding scattering centers. In the hyper-netted chain closure approximation (HNC) this reads

$$\begin{aligned} V^{MF,cl}(r) &= V(r) - \frac{1}{\beta} (h(r) - C(r)) \\ &= V(r) + n^0 \int d^3r' \frac{C(|\mathbf{r} - \mathbf{r}'|)}{-\beta} h(r') \end{aligned} \quad (25)$$

where  $h(r)$  is the pair correlation function<sup>3</sup>,  $C(r)$  the direct correlation function,  $n^0$  is the particle density,  $V(r)$  the direct interaction potential between two particles (e.g. the coulomb potential), and  $\beta$  is the inverse temperature. Such a mean field potential has been used successfully for calculation of ionic transport quantities [24, 31]. The analogous electron-ion potential when considering quantal electrons is given by the quantum Ornstein-Zernike equations as [25, 32]

$$V^{MF}(r) = V_{ie}(r) + n_i^0 \int d^3r' \frac{C_{ie}(|\mathbf{r} - \mathbf{r}'|)}{-\beta} h_{ii}(r') \\ + \bar{n}_e^0 \int d^3r' \frac{C_{ee}(|\mathbf{r} - \mathbf{r}'|)}{-\beta} h_{ie}(r') \quad (26)$$

where  $C_{ie}$  ( $C_{ee}$ ) is the electron-ion (-electron) direct correlation function. The quantum Ornstein-Zernike equations are valid when the electrons respond linearly to the ions, i.e. in the linear response regime. Thus is it necessary to artificially separate the electrons into two groups: those that are bound the nucleus ( $n_e^{ion}(r)$ ) and therefore respond very non-linearly, and those that are not bound ( $n_e^{scr}(r)$ ), and for which linear response is reasonably accurate. This was the approach taken in [33, 34] where the quantum Ornstein-Zernike equations were solved and resulting pair distribution functions were shown to be accurate. Adopting that model,  $V_{ie}(r)$  becomes

$$V_{ie}(r) = -\frac{Z}{r} + \int d^3r' \frac{n_e^{ion}(r')}{|\mathbf{r} - \mathbf{r}'|} + V^{xc}[n_e^{ion}(r)] \quad (27)$$

Using the relation [33]

$$C_{ij}(k) = -\beta V_{ij}^C(k) + \tilde{C}_{ij}(k) \quad (28)$$

where  $V_{ij}^C(k) = Z_i Z_j 4\pi/k^2$  is the Coulomb potential in Fourier Space between two charges  $Z_i$  and  $Z_j$ , and collecting terms gives

$$V^{MF}(r) = V^{PA}(r) + n_i^0 \int d^3r' \frac{\bar{Z} h_{ii}(r') + n_e^{ext}(r')}{|\mathbf{r} - \mathbf{r}'|} \\ + V^{xc}[n_e^{ext}(r)] \\ + n_i^0 \int d^3r' \frac{\tilde{C}_{ie}(|\mathbf{r} - \mathbf{r}'|)}{-\beta} h_{ii}(r') \quad (29)$$

with

$$n_e^{ext}(r) = \int d^3r' n_e^{scr}(r') h_{ii}(|\mathbf{r} - \mathbf{r}'|) \quad (30)$$

and  $\bar{Z} = \bar{n}_e^0/n_i^0 = \int d^3r n_e^{scr}(r)$ .  $V^{MF}(r)$  is the scattering potential for one scattering center, and implicitly includes the ionic structure ( $S_{ii}(q) = 1 + n_i^0 h_{ii}(q)$ ), i.e.

<sup>3</sup>  $h(r)$  is simply related the structure factor  $S(q) = 1 + n^0 h(q)$ .

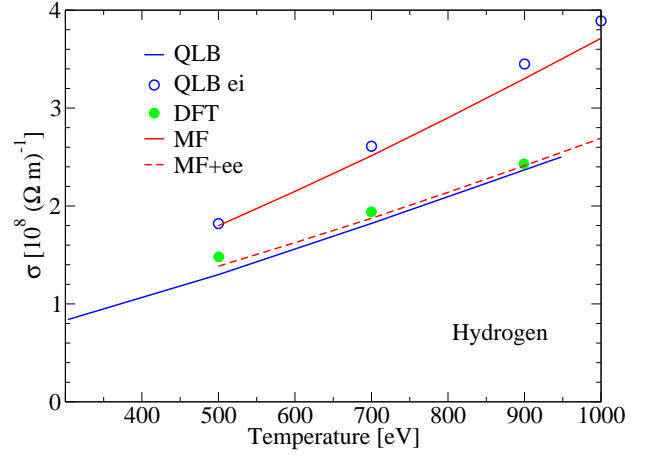


FIG. 2: (Color online) The effect of electron-electron collisions on the electrical conductivity of hydrogen at 40 g/cm<sup>3</sup>. Compare with figure 3a of reference [6]. Our calculations using the mean force potential (MF) agree well with the quantum Lenard-Balescu calculations with only electron-ion collisions included (QLB ei). Including a correction factor that accounts for electron-electron collisions due to Reinholz *et al* [26], our calculations (MF+ee) fall into close agreement with the QLB calculation that include electron-electron collisions, as well as DFT simulation results.

$S_{ii}(q)$  does not explicitly appear as in equations (22) and (24) for the pseudoatom and average atom differential cross sections. Hence, the angular integral in equation (10) can be carried out analytically and we directly solve equation (13).

In the high temperature regime  $h_{ii}(r) \rightarrow 0 \forall r$ , and  $\tilde{C}_{ie}(r) \rightarrow 0 \forall r$ , hence  $V^{MF}(r) \rightarrow V^{PA}(r)$ , and the Born limit will be recovered.

It is interesting to note that the potential of mean force obtained above (equation (26)) is that same as the potential used in Chihara's QHNC model [25]. There it has not been used for conductivity calculations.

In figure 1 examples of these three potentials  $V^{AA}(r)$ ,  $V^{MF}(r)$  and  $V^{PA}(r)$  are shown for aluminum at 2 eV and 2.7 g/cm<sup>3</sup> (top panel) and 0.1 g/cm<sup>3</sup> (bottom panel). For the higher density case correlations are important and  $V^{MF}(r)$  is close to  $V^{AA}(r)$ , whereas for the lower density case correlations are less important and  $V^{MF}(r)$  is closer to  $V^{PA}(r)$ .

### III. NUMERICAL RESULTS

To generate the potentials needed for calculation of the conductivities ( $V^{AA}(r)$ ,  $V^{PA}(r)$  and  $V^{MF}(r)$ ) we have used the model of references [33, 34]. In this model DFT is used to determine the electronic structure of one average atom in the plasma. This provides a closure relation for the quantum Ornstein Zernike equations, which are thus solved self-consistently for all quantities of interest

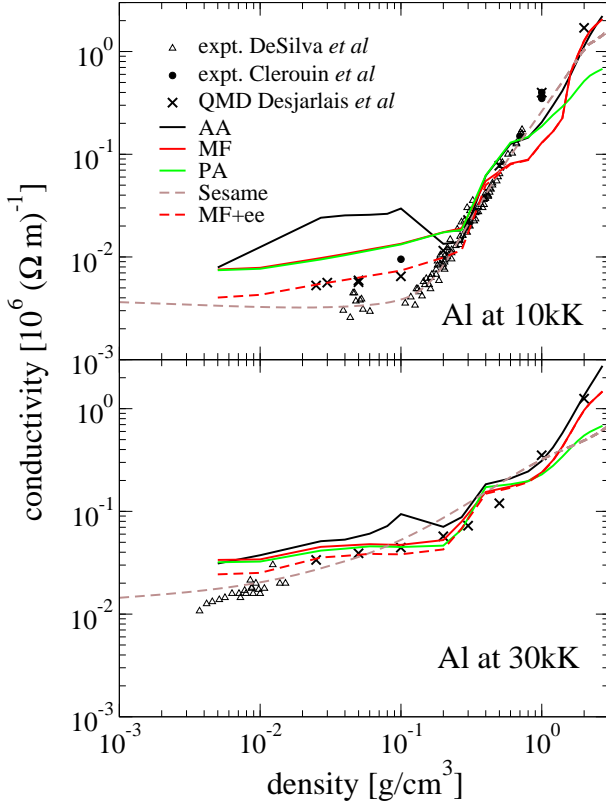


FIG. 3: (Color online) Electrical conductivity of aluminum at 10 kK (top panel) and 30 kK (bottom panel) as calculated in the present approach for the three potentials  $V^{AA}(r)$ ,  $V^{PA}(r)$  and  $V^{MF}(r)$ . Comparisons are made to QMD simulations of Desjarlais *et al* [1] and to the experiments of DeSilva *et al* [8] and Cl  rouin *et al* [9]. MF+ee refers to calculation using  $V^{MF}(r)$  and explicitly accounting for electron-electron collisions using the fit formula of reference [26].

(eg.  $S_{ii}(k)$ ,  $C_{ie}(k)$ ,  $\bar{n}_e^0$  etc.) This model has been shown to be realistic for equation of state [36] and ionic structure [37]. It is a plasma model, and as such is most accurate at elevated temperatures. For example, for aluminum at solid density realistic structure factors were predicted for temperatures greater than  $\sim 1$  eV [33]. A numerical issue for the solution of equation (13) at very high temperatures is discussed in the appendix.

The conductivity model discussed in section II includes electron collisions with ions in the plasma. There is no explicit account of electron-electron collisions. This difficult problem has been discussed by a number of authors [6, 26, 38–40]. Here we test the effect of including electron-electron collisions by using the fit formula due to Reinholz *et al* [26]. This formula takes as input the ion density, temperature and the average ionization (which is provided by the model of references [33, 34]). Very recently, the effect of electron-electron collisions on electrical conductivity was considered in detail [6] by comparing quantum Lenard-Balescu calculations that explicitly account for both electron-electron and electron-ion

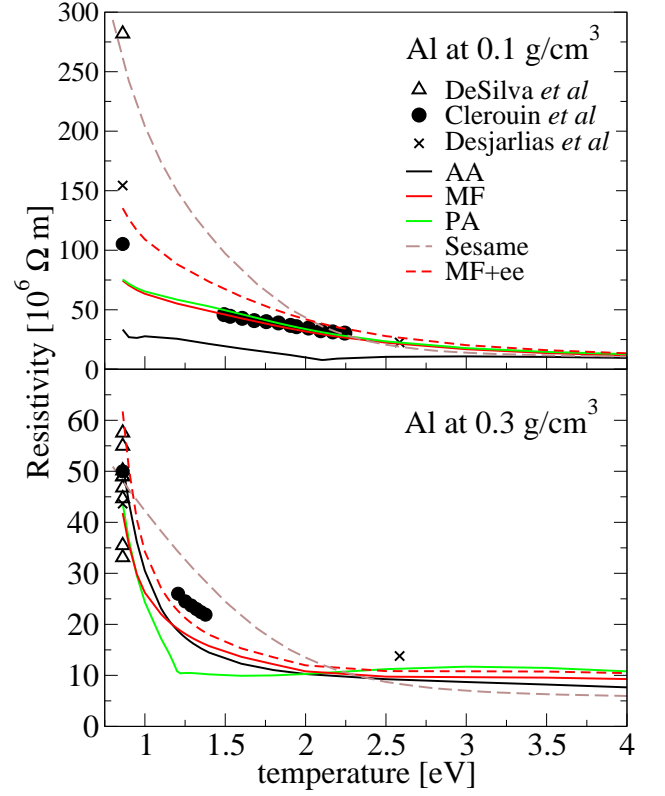


FIG. 4: (Color online) Electrical resistivity of aluminum at  $0.1 \text{ g/cm}^3$  (top panel) and  $0.3 \text{ g/cm}^3$  (bottom panel). Experiments are from Cl  rouin *et al* [10] and DeSilva *et al* [8]. Also shown are DFT-MD (QMD) results of Desjarlais *et al* [1]. Present results use the three potentials discussed in the text:  $V^{AA}(r)$ ,  $V^{PA}(r)$  and  $V^{MF}(r)$ , as well as the effect of electron-electron collisions for  $V^{MF}(r)$  (MF+ee). Also shown is Sesame 29371 which is based on the models of references [13, 35].

collisions, to DFT-MD simulations that use the Kubo-Greenwood formalism. In figure 2 we compare to the results of reference [6] for hot, dense hydrogen. From the figure it is clear that including only electron-ion collisions in the present method leads to good agreement with the QLB results that also only include electron-ion collisions. Adding the electron-electron collisions factor to the mean force results, we now see agreement with the QLB collision that also explicitly account for these, as well as good agreement with the DFT results. This comparison strongly indicates that it is necessary to explicitly account of electron-electron collisions in our relaxation time approach.

In figure 3 we compare to the experiments of references [8] and [9] for aluminum at two temperatures (10 kK and 30 kK) as a function of density. We also show DFT-MD (also known as QMD) results from reference [1], which is a less approximate method than the present, but is much more computationally expensive. Results using  $V^{AA}(r)$  are in reasonable agreement with the QMD

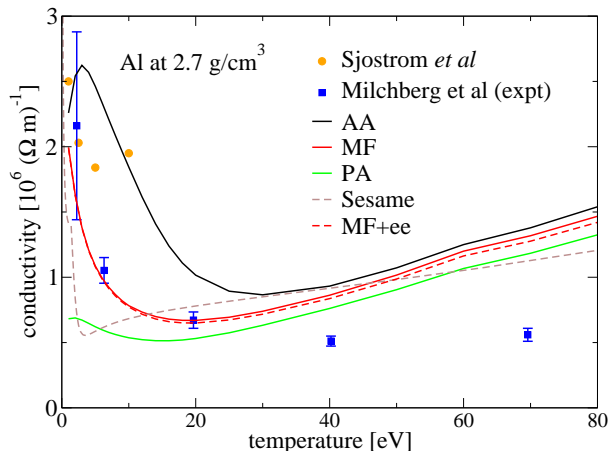


FIG. 5: (Color online) Electrical conductivity of aluminum at  $2.7 \text{ g/cm}^3$  as calculated in the present approach for the three potentials  $V^{AA}(r)$ ,  $V^{PA}(r)$  and  $V^{MF}(r)$ , compared to the experiment of Milchberg *et al* [11]. Also shown are DFT-MD results due to Sjostrom *et al* [2] and Sesame 29371.

calculations at high densities, but tend to be too large at lower densities, compared to the experimental data. In contrast,  $V^{PA}(r)$  gives reasonable results at lower densities, but underestimates the QMD results at high densities.  $V^{MF}(r)$  gives reasonable, but not perfect, agreement at both low and high densities, for both temperatures. Including the electron-electron collision factor, agreement with the experiment and the DFT-MD simulations for the mean force potential is markedly improved. This further strengthens the case that electron-electron collisions should be explicitly accounted for when using the relaxation time approach. We note that the correction factor is the same for all three potentials, but its effect is only shown for  $V^{MF}(r)$  for clarity.

It should also be noted that the range of conditions plotted in figure 3 is a particularly challenging regime to model due to the relocation of electrons as density is lowered. This relocation explains the structures in the present results, which are a consequence of the spherical symmetry in the underlying model [33, 34], and are probably too pronounced. Also shown in the figure are Sesame 29371 curves, which were designed to fit the experiments [8] and as a consequence agree very well with those experiments. At the highest densities shown, the Sesame curve underestimates the QMD calculations, particularly at 30 kK.

In figure 4 calculations of the resistivity of warm dense aluminum at  $0.1 \text{ g/cm}^3$  and  $0.3 \text{ g/cm}^3$  are compared to the experimental results of Cl  rouin *et al* [9, 10] and DeSilva *et al* [8] as well as DFT-MD results from reference [1]. Results using all three types of potential are shown. All the theory curves are reasonably close to each other for temperatures greater than 2 eV. For temperatures lower than this the variance significantly increases. Compared to the Cl  rouin *et al* data the mean-force potential

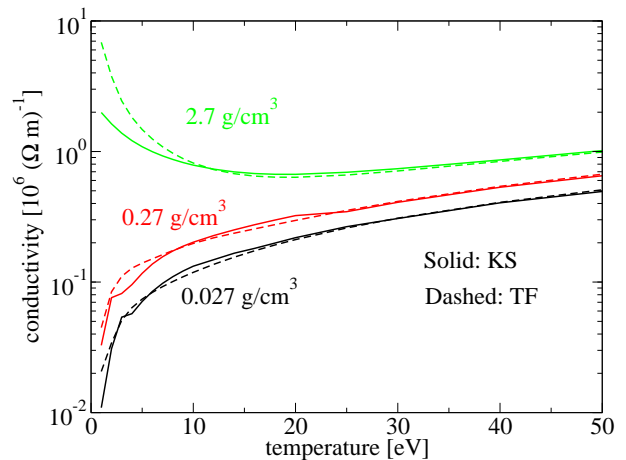


FIG. 6: (Color online) Electrical conductivity of aluminum using the  $V^{MF}(r)$  potential (no electron-electron factor). Results using a potential created by a Kohn-Sham calculation are compared to those created using a Thomas-Fermi calculation for three densities. For the cases shown the two calculations agree well for temperatures greater than roughly 25 eV.

gives reasonable agreement for both densities, whereas neither  $V^{AA}(r)$  or  $V^{PA}(r)$  give a consistent level of agreement with the data at both densities.  $V^{AA}(r)$  is closer to the data at the higher density, where correlations with surrounding ions are relatively important, while  $V^{PA}(r)$  is closer at the lower density, where the influence of correlations is reduced. While the agreement of the  $V^{MF}$  calculations is not perfect it should be remembered that neither is the underlying model [33, 34] or the experiments, which themselves do not agree with each other. The effect of electron-electron collisions is significant in for the lower temperatures. We note that the temperatures of the experiments of Cl  rouin *et al* are obtained through comparison with DFT-MD simulations [10] and are not measured directly. For completeness we have also compared to Sesame calculations that are based on the model of [35]. The Sesame result tends to overestimate the Cl  rouin *et al* data. They are fit to the DeSilva *et al* data [35] and are therefore in good agreement with those experiments.

In figure 5 we compare to the experiment of reference [11]. This experiment reported results for solid density aluminum up to high temperatures. We also compare to DFT-MD results from reference [2]. At the lower temperatures (20 eV and below) the results using  $V^{MF}(r)$  agree well with the experiment. They underestimate the DFT-MD results of [2] by  $\sim 20\%$  at 1 eV. Note that the increase in conductivity in going from 5 to 10 eV reported by Sjostrom *et al* [2] may be an artifact of the pseudopotential used [41]. The  $V^{PA}(r)$  results significantly underestimate the conductivity in the low temperature regime compared to both the DFT-MD and experimental results. The  $V^{AA}(r)$  results over predict the conductivity



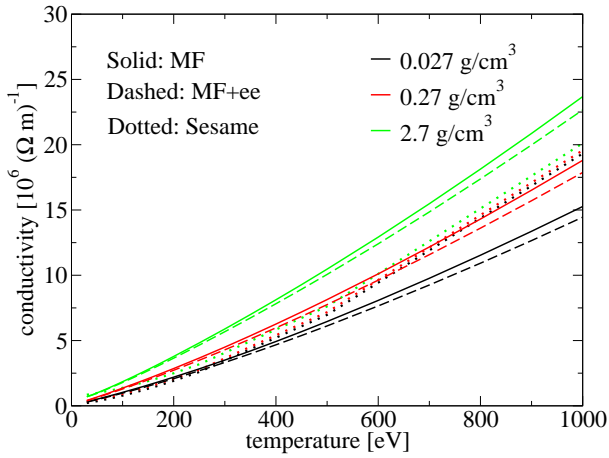


FIG. 7: (Color online) Electrical conductivity of aluminum using the  $V^{MF}(r)$  potential compared to Sesame 29371 [13, 35]. The mean force calculations suggest that conductivity is significantly more sensitive to density than the Sesame model indicates.

in this regime. At higher temperatures none of the results from the potentials match the experiment. However, it has been pointed out [42] that the temperatures reported in [11] are dependent on a model for ionization, and that different models yield significantly different temperatures (eg. the 40 eV point becomes 23.5eV). Moreover, while dc conductivity was reported, it as an ac conductivity at 4.026 eV that was measured. Finally, we also show the Sesame result. This curve has a much sharper drop at low temperatures, and a different slope as temperature is increased. Over the temperature range shown the maximum difference between Sesame and the  $V^{MF}(r)$  curve is a factor of  $\sim 2$ , but is generally closer. The effect of electron-electron collisions is small due to the relatively high degeneracy of the plasma and relatively large electron-ion collision cross section.

While generation of the potential  $V^{MF}(r)$  using the model of references [33, 34] is computationally inexpensive relative to DFT-MD simulations, it still takes 30 minutes to 1 hour per density temperature point. With a view to generating tables of conductivity data it is desirable to find an even more computationally efficient model. One option is to use a Thomas-Fermi based DFT model, in place of the Kohn-Sham description used above [33, 34]. With such a model it takes seconds to generate  $V^{MF}(r)$ . In figure 6 we compare conductivities using the Kohn-Sham and Thomas-Fermi methods of generating  $V^{MF}(r)$ . We find that for the densities shown the Thomas-Fermi and Kohn-Sham results agree very closely for temperature greater than 25 eV. The Thomas-Fermi model therefore offers a rapid shortcut to realistic potentials for sufficiently high temperatures.

In figure 7 we compare calculations based on the present  $V^{MF}(r)$  model to the Sesame table 29371, based on the model of [13, 35], up to 1000 eV. We find that the

present model shows much more sensitivity to density than Sesame 29371 does and that the effect of electron-electron collisions remains relatively small even at these high temperatures. At 1000 eV the present model is  $\sim 13\%$  larger for  $2.7 \text{ g/cm}^3$ , while at  $0.027 \text{ g/cm}^3$ , the present model gives conductivities  $\sim 25\%$  lower.

#### IV. CONCLUSIONS

We have presented a potential of mean force that, coupled with the relaxation time approximation, is used to calculate electrical conductivity of dense plasmas. Compared to previously used potentials we found improved agreement with experiments and bench mark calculations across a range of temperatures and densities for aluminum. We note that the new potential takes into account the self-consistent ionic structure factor implicitly, in contrast to other methods where the structure factor appears explicitly. This is important because to generate the potential of mean force, one needs a model that self-consistently solves the quantum Ornstein Zernike equations, whereas previously the scattering potential and structure factor have often been generated by distinct models.

In applying the new model the influence of electron-electron collisions was included using the fit formula of reference [26]. It was found that for dense hydrogen this was essential for agreement with other methods that are thought to be accurate, indicating the importance and correctness of their inclusion. In comparison with experiments on aluminum by DeSilva *et al* [8], it was found that inclusion of electron-electron collisions significantly improved agreement with both the experiments and bench mark calculations.

We also tested the effect of generating the potential of mean force with a Thomas-Fermi DFT based model as opposed to the more accurate Kohn-Sham DFT calculation. It was found that for aluminum from  $0.027$  to  $2.7 \text{ g/cm}^3$  the TF based model was accurate for temperatures greater than  $\sim 25 \text{ eV}$ , a fact that greatly speeds up the calculations. It is important to realise that while the potential can be generated using the TF based model, the conductivity itself is based on a calculation of the phase shifts in the usual way.

The new method was compared to Sesame table 29371 for aluminum and was found to have a significantly greater dispersion with respect to density at high temperature than Sesame. At low temperatures significant differences (up to a factor of  $\sim 2$ ) were also observed.

While we have demonstrated that the new potential results in generally improved agreement with bench mark calculations and experiments, the model as a whole is not perfect and could be further improved in a number of ways. Perhaps the most apparent error is that the potential assumes on average ionic configuration, instead of a weighted range of configurations. This leads to structures in the conductivity as a function of density and

temperature that are likely to be too pronounced. This predominately effects the lower densities and temperatures considered here. Other potential sources of error or uncertainty include the influence of a more realistic density of states factor [36], or the choice of exchange and correlation potential in the underlying DFT calculation [17].

We have focused mainly of aluminum, for which most experimental data is available, but there is no fundamental restriction and the method should be applicable other materials. Also, it is straightforward to extend to the calculation of thermal conductivity. However, recent investigations [6] point to the need for care with such calculation with respect to the inclusion of electron-electron collisions. Finally, we point out that this new potential is also applicable to opacity calculations [43] where it could aid in the assessment of the influence of ionic structure on opacity [44].

### Acknowledgments

The author acknowledges useful conversations with S. Baalrud and thanks T. Sjoström for providing his DFT-MD data and M. Desjarlais for useful comments on the manuscript. This work was performed under the auspices of the United States Department of Energy under contract DE-AC52-06NA25396.

### Appendix A: Calculation of phase shifts

Calculation of the scattering amplitudes requires the scattering phase shifts  $\eta_l(\epsilon)$  for the potential. These are

calculated in the usual way via continuum state normalization. However, high plasma temperatures and low densities require phase shifts at large  $l$  ( $> 10000$  are required) and  $\epsilon$  (up to  $\sim 1000 E_h$ ). Such cases are numerically more challenging and a number of schemes have been proposed to circumvent their calculation [18, 27]. We have implemented a different scheme that we found to be accurate and reliable.

The phase shifts are calculated in the semi-classical JWKB approximation with knowledge only of the scattering potential [45]

$$\eta_l(\epsilon) = \int_{R_C}^{\infty} \left[ p^2 - 2V^{scatt}(r) - \frac{(l + \frac{1}{2})^2}{r^2} \right]^{\frac{1}{2}} dr - \int_{(l + \frac{1}{2})/p}^{\infty} \left[ p^2 - \frac{(l + \frac{1}{2})^2}{r^2} \right]^{\frac{1}{2}} dr \quad (A1)$$

where  $R_C$  is the classical turning point which restricts the integrand of the first integral to be positive energy

$$p^2 - 2V(R_C) - (l + \frac{1}{2})^2 R_C^{-2} = 0 \quad (A2)$$

We have found this calculation to be fast, accurate and stable even for very large  $l$  ( $> 30000$ ). Typically we switch to this calculation for energies greater than  $50 E_h$  or orbital angular momenta greater than 30.

- 
- [1] M. P. Desjarlais, J. D. Kress, and L. A. Collins. Electrical conductivity for warm, dense aluminum plasmas and liquids. *Phys. Rev. E*, 66:025401, Aug 2002.
  - [2] Travis Sjoström and Jérôme Daligault. Ionic and electronic transport properties in dense plasmas by orbital-free density functional theory. *Phys. Rev. E*, 92:063304, 2015.
  - [3] Bastian Holst, Martin French, and Ronald Redmer. Electronic transport coefficients from *ab initio* simulations and application to dense liquid hydrogen. *Phys. Rev. B*, 83:235120, Jun 2011.
  - [4] Martin French and Thomas R Mattsson. Thermoelectric transport properties of molybdenum from *ab initio* simulations. *Physical Review B*, 90(16):165113, 2014.
  - [5] S. X. Hu, L. A. Collins, T. R. Boehly, J. D. Kress, V. N. Goncharov, and S. Skupsky. First-principles thermal conductivity of warm-dense deuterium plasmas for inertial confinement fusion applications. *Phys. Rev. E*, 89:043105, Apr 2014.
  - [6] Michael P. Desjarlais, Christian R. Scullard, Lorin X. Benedict, Heather D. Whitley, and Ronald Redmer. Density-functional calculations of transport properties in the nondegenerate limit and the role of electron-electron scattering. *Phys. Rev. E*, 95:033203, Mar 2017.
  - [7] P. Sperling, E. J. Gamboa, H. J. Lee, H. K. Chung, E. Galtier, Y. Omarbakiyeva, H. Reinholz, G. Röpke, U. Zastra, J. Hastings, L. B. Fletcher, and S. H. Glenzer. Free-electron x-ray laser measurements of collisional-damped plasmons in isochorically heated warm dense matter. *Phys. Rev. Lett.*, 115:115001, 2015.
  - [8] A. W. DeSilva and J. D. Katsourous. Electrical conductivity of dense copper and aluminum plasmas. *Phys. Rev. E*, 57:5945–5951, May 1998.
  - [9] Jean Clérouin, Pierre Noiret, Victor N. Korobenko, and Anatoly D. Rakhel. Direct measurements and *ab initio* simulations for expanded fluid aluminum in the metal-nonmetal transition range. *Physical Review B*, 78(22):224203, 2008.
  - [10] J. Clérouin, P. Noiret, P. Blottiau, V. Recoules, B. Siberchicot, P. Renaudin, C. Blancard, G. Faussurier, B. Holst, and C. E. Starrett. A database for equations of state and resistivities measurements in the warm dense matter regime. *Physics of Plasmas*, 19(8):082702, 2012.
  - [11] H. M. Milchberg, R. R. Freeman, S. C. Davey, and R. M.



- More. Resistivity of a simple metal from room temperature to  $10^6$  K. *Phys. Rev. Lett.*, 61:2364–2367, Nov 1988.
- [12] J. F. Benage, W. R. Shanahan, and M. S. Murillo. Electrical resistivity measurements of hot dense aluminum. *Phys. Rev. Lett.*, 83:2953–2956, Oct 1999.
- [13] Yim T. Lee and R. M. More. An electron conductivity model for dense plasmas. *The Physics of fluids*, 27(5):1273–1286, 1984.
- [14] D.J. Burrill, D.V. Feinblum, M.R.J. Charest, and C.E. Starrett. Comparison of electron transport calculations in warm dense matter using the ziman formula. *High Energy Density Physics*, 19:1 – 10, 2016.
- [15] J.M. Ziman. A theory of the electrical properties of liquid metals. i: The monovalent metals. *Philosophical Magazine*, 6(68):1013–1034, 1961.
- [16] George A. Rinker. Systematic calculations of plasma transport coefficients for the periodic table. *Phys. Rev. A*, 37:1284–1297, 1988.
- [17] A.A. Ovechkin, P.A. Loboda, and A.L. Falkov. Transport and dielectric properties of dense ionized matter from the average-atom reaos model. *High Energy Density Physics*, 20:38 – 54, 2016.
- [18] François Perrot and M. W. C. Dharma-wardana. Electrical resistivity of hot dense plasmas. *Phys. Rev. A*, 36:238–246, Jul 1987.
- [19] Gérald Faussurier, Christophe Blancard, Philippe Cossé, and Patrick Renaudin. Equation of state, transport coefficients, and stopping power of dense plasmas from the average-atom model self-consistent approach for astrophysical and laboratory plasmas. *Physics of Plasmas*, 17(5), 2010.
- [20] P.A. Sterne, S.B. Hansen, B.G. Wilson, and W.A. Isaacs. Equation of state, occupation probabilities and conductivities in the average atom purgatorio code. *High Energy Density Physics*, 3(12):278 – 282, 2007. Radiative Properties of Hot Dense Matter.
- [21] C. E. Starrett, J Clérouin, V Recoules, J. D. Kress, L. A. Collins, and D. E. Hanson. Average atom transport properties for pure and mixed species in the hot and warm dense matter regimes. *Physics of Plasmas (1994-present)*, 19(10):102709, 2012.
- [22] François Perrot and M.W.C. Dharma-Wardana. Theoretical issues in the calculation of the electrical resistivity of plasmas. *International journal of thermophysics*, 20(4):1299–1311, 1999.
- [23] Charles Edward Starrett. Kubo–greenwood approach to conductivity in dense plasmas with average atom models. *High Energy Density Physics*, 19:58–64, 2016.
- [24] Scott D. Baalrud and Jérôme Daligault. Effective potential theory for transport coefficients across coupling regimes. *Phys. Rev. Lett.*, 110:235001, Jun 2013.
- [25] Junzo Chihara. Unified description of metallic and neutral liquids and plasmas. *Journal of Physics: Condensed Matter*, 3(44):8715, 1991.
- [26] H. Reinholz, G. Röpke, S. Rosmej, and R. Redmer. Conductivity of warm dense matter including electron-electron collisions. *Physical Review E*, 91(4):043105, 2015.
- [27] J.C. Pain and G. Dejonghe. Electrical resistivity in warm dense plasmas beyond the average-atom model. *Contributions to Plasma Physics*, 50(1):39–45, 2010.
- [28] Gérald Faussurier and Christophe Blancard. Resistivity saturation in warm dense matter. *Phys. Rev. E*, 91:013105, Jan 2015.
- [29] Balazs F. Rozsnyai. Electron scattering in hot/warm plasmas. *High Energy Density Physics*, 4(1):64–72, 2008.
- [30] R. Evans, B. L. Gyorfey, N. Szabo, and J. M. Ziman. On the resistivity of liquid transition metals. In S. Takeuchi, editor, *The properties of liquid metals*. Taylor and Francis, London, 1973.
- [31] Jérôme Daligault, Scott D. Baalrud, Charles E. Starrett, Didier Saumon, and Travis Sjostrom. Ionic transport coefficients of dense plasmas without molecular dynamics. *Physical review letters*, 116(7):075002, 2016.
- [32] C. E. Starrett, D. Saumon, J. Daligault, and S. Hamel. Integral equation model for warm and hot dense mixtures. *Physical Review E*, 90(3):033110, 2014.
- [33] C. E. Starrett and D. Saumon. Electronic and ionic structures of warm and hot dense matter. *Phys. Rev. E*, 87:013104, Jan 2013.
- [34] C.E. Starrett and D. Saumon. A simple method for determining the ionic structure of warm dense matter. *High Energy Density Physics*, 10:35 – 42, 2014.
- [35] M.P. Desjarlais. Practical improvements to the lee-more conductivity near the metal-insulator transition. *Contributions to Plasma Physics*, 41(2-3):267–270, 2001.
- [36] C. E. Starrett and D. Saumon. Equation of state of dense plasmas with pseudoatom molecular dynamics. *Phys. Rev. E*, 93:063206, Jun 2016.
- [37] C. E. Starrett and D. Saumon. Models of the elastic x-ray scattering feature for warm dense matter. *Phys. Rev. E*, 92:033101, 2015.
- [38] A. Yu Potekhin and D.G. Yakovlev. Electron conduction along quantizing magnetic fields in neutron star crusts. ii. practical formulae. *Astronomy and Astrophysics*, 314:341–352, 1996.
- [39] S. Kuhlbrodt, R. Redmer, A. Kemp, and J. Meyer-ter Vehn. Conductivities in hot aluminium plasma. *Contributions to Plasma Physics*, 41(1):3–14, 2001.
- [40] M.W.C. Dharma-Wardana. Static and dynamic conductivity of warm dense matter within a density-functional approach: Application to aluminum and gold. *Physical Review E*, 73(3):036401, 2006.
- [41] T. Sjostrom. *Private communication*.
- [42] M.W.C. Dharma-Wardana and François Perrot. Resistivity and dynamic conductivity of laser-pulse heated aluminum up to 106 K and along the shock hugoniot up to 20 mbars. *Physics Letters A*, 163(3):223–227, 1992.
- [43] Nathaniel R. Shaffer, Natalie G. Ferris, J. Colgan, David Parker Kilcrease, and Charles Edward Starrett. Free-free opacity in dense plasmas with an average atom model. *High Energy Density Physics*, 23:31–37, 2017.
- [44] Menahem Krief, Yair Kurzweil, Alexander Feigel, and Doron Gazit. The effect of ionic correlations on radiative properties in the solar interior and terrestrial experiments. *arXiv preprint arXiv:1611.09339*, 2016.
- [45] G. W. F. Drake (Editor). *Springer handbook of atomic, molecular and optical physics*. Springer, 2005.